

SWITCHGRASS GENOTYPE CLASSIFICATION USING HYPERSPECTRAL IMAGERY

By

HUDANYUN SHENG

A THESIS PRESENTED TO THE GRADUATE SCHOOL  
OF THE UNIVERSITY OF FLORIDA IN PARTIAL FULFILLMENT  
OF THE REQUIREMENTS FOR THE DEGREE OF  
MASTER OF SCIENCE

UNIVERSITY OF FLORIDA

2019

© 2019 Hudanyun Sheng

To the very best of times! To the days and nights in either lab or gym! To coffee and pizza!

## ACKNOWLEDGMENTS

I would like to thank my dearest advisor, Dr. Alina Zare, for all her guidance, support and opportunities she provided with me throughout my studies and research. I would also like to thank my committee members, Dr. Paul Gader, and Dr. Damon Woodard, for all their help and valuable suggestions.

I would also like to express my sincere gratitude to Dr. Brandon Davis, Dr. Felix Fritschi and Ms. Hannah Wilson for their dedicated work on data collection and numerous advices and discussions with me.

Additionally thank you my labmates. I am particularly thankful to Weihuang Xu and Guohao Yu for their patience and willingness of offering help.

Finally many thanks Dr. Panos M. Pardalos, whose course first made me feel like digging into the world of Machine Learning.

## TABLE OF CONTENTS

	<u>page</u>
ACKNOWLEDGMENTS . . . . .	4
LIST OF TABLES . . . . .	7
LIST OF FIGURES . . . . .	8
ABSTRACT . . . . .	9
CHAPTER	
1 INTRODUCTION . . . . .	11
1.1 Goal of Study . . . . .	11
1.2 Hyperspectral Imaging and Application . . . . .	11
1.3 Classification in High Dimensional Space . . . . .	12
1.4 Statement of the problem . . . . .	13
2 LITERATURE REVIEW . . . . .	14
2.1 Stitching and Making Orthomosaics . . . . .	14
2.2 Hyperspectral Unmixing . . . . .	15
2.3 Classification in High Dimensional Space . . . . .	18
3 MATERIALS AND METHODS . . . . .	20
3.1 Dataset . . . . .	20
3.2 Switchgrass Detection . . . . .	20
3.2.1 Sparsity Promoting Iterated Constrained Endmember Detection (SPICE) . . . . .	20
3.2.2 Switchgrass Detection generation . . . . .	22
3.3 Switchgrass Genotype Classification . . . . .	23
3.3.1 Dimensionality Reduction by Learning an Invariant Mapping . . . . .	23
3.3.2 K Nearest Neighbor Classifier . . . . .	25
3.3.3 Ground Truth Generation . . . . .	25
3.4 Summary of Proposed Approach . . . . .	25
4 RESULTS . . . . .	27
4.1 Preprocessing of hyperspectral images . . . . .	27
4.1.1 Radiometric Calibration . . . . .	27
4.1.2 Stitching and Making Orthomosaics . . . . .	27
4.1.3 Noisy Band Removal . . . . .	28
4.2 Detection of Switchgrass . . . . .	29
4.2.1 Hyperspectral endmember detection and unmixing . . . . .	29
4.2.2 Ground truth labeling . . . . .	30
4.2.3 Final detection generation . . . . .	30
4.3 Switchgrass Classification Results . . . . .	34

4.3.1	Siamese Network Training . . . . .	35
4.3.2	Classification . . . . .	36
5	SUMMARY AND CONCLUSIONS . . . . .	41
	REFERENCES . . . . .	43
	BIOGRAPHICAL SKETCH . . . . .	47

## LIST OF TABLES

<u>Table</u>		<u>page</u>
4-1 Average classification accuracy of training folds. . . . .		37

## LIST OF FIGURES

<u>Figure</u>	<u>page</u>
1-1 Graphic representation of a hyperspectral cube and sample hyperspectral spectra . . . . .	12
3-1 Toy example of the data and the simplex shown in two-dimensional space. . . . .	21
3-2 Contrastive loss function representation and the network architecture. . . . .	24
3-3 The flowchart of the adopted approach. . . . .	26
4-1 Radiometric Calibration . . . . .	27
4-2 Stitched images from one example scanning of the STND switchgrass field. . . . .	28
4-3 Sample spectra before and after noisy band removal. . . . .	29
4-4 Detected endmembers using SPICE algorithm. . . . .	30
4-5 Abundance maps and original hyperspectral image for GWAS field. . . . .	31
4-5 Abundance maps and original hyperspectral image for STND field. . . . .	33
4-6 Example of manual labeling the ground truth interactively using MATLAB. . . . .	33
4-7 Abundance maps and original hyperspectral image for STND field. . . . .	34
4-8 Learning curve for Siamese network training. . . . .	35
4-9 Siamese network model selection. . . . .	36
4-10 Classification performance of switchgrass pixels for all test data from training images.	37
4-11 Classification performance of switchgrass pixels for all pixels from all test images. . .	38
4-12 Sample classification result shown in images. . . . .	39
4-12 Original spectra and dimensionality reduction result. . . . .	40

Abstract of Thesis Presented to the Graduate School  
of the University of Florida in Partial Fulfillment of the  
Requirements for the Degree of Master of Science

SWITCHGRASS GENOTYPE CLASSIFICATION USING HYPERSPECTRAL IMAGERY

By

Hudanyun Sheng

December 2019

Chair: Alina Zare

Major: Electrical and Computer Engineering

The adoption of remote sensing techniques in plant science enables the noninvasive or minimally invasive technologies, as well as the time and labor saving from the traditional field measurements. A method to learn the properties of switchgrass with only the analysis of hyperspectral imagery instead of tedious and time-consuming field measurements is proposed.

A processing protocol of hyperspectral imagery including preprocessing, hyperspectral image ortho-mosaic generation, hyperspectral endmember detection, hyperspectral unmixing and pixel-level genotype classification is presented. A combined machine learning algorithm for material detection, dimensionality and classification is proposed and discussed in detail.

Target detection is a promising application of hyperspectral imagery owing to its high spectral resolution. In the meantime, the spectra in hyperspectral images are mixtures of spectra of various materials in the scene due to its low spatial resolution of hyperspectral sensors. Hyperspectral unmixing, including estimating of number of endmembers, the spectral signatures of endmembers, as well as generating the abundances of every endmember at each pixel, is necessary for target detection. In this work, the detection of switchgrass is realized by hyperspectral unmixing using Sparsity Promoting Iterated Constrained Endmember Detection (SPICE) algorithm. Different from other hyperspectral endmember detection algorithms, the SPICE algorithm is able to estimate the number of endmembers automatically by using a sparsity-promoting prior.

The curse of dimensionality limits the application of high dimensional data so that dimensionality reduction is often adopted as a preprocessing step. Siamese network, the dimensionality reduction algorithm adopted in this work, learns a mapping from the original space to a low dimensional manifold such that data originally from different classes are far away from each other while data originally from the same class stay close to each other.

K-nearest neighbor (KNN) is used as multi-class classifier in this work. KNN is one of the simplest non-parametric supervised classification algorithms which assumes that similar data points exist in close proximity and the output of the dimensionality reduction has this characteristic.

Results show that the SPICE algorithm consistently learns the endmembers of switchgrass, as well as other materials in scene. The switchgrass detection is fulfilled by unmixing. When trying to distinguish different genotypes of a same plant species, unmixing no longer works because their spectra are not distinguishable. The Siamese network shows the capability of reducing the dimensionality and distinguish the differences among genotypes.

## CHAPTER 1

### INTRODUCTION

#### 1.1 Goal of Study

Switchgrass, also known as *panicum virgatum*, is one of the dominant species native to North America. Switchgrass can be used as feedstock for biomass energy production, ground cover for soil conservation to control erosion, or grazing. Different genotypes of switchgrass behave differently regarding height, tiller counts, dry biomass weight. Plant phenotyping tries to quantitatively measure the structural and functional properties of different genotypes of plants and selects the genotypes best suit the desired application. Traditional phenotyping methods are laborious and time-consuming ([Mahlein, 2016](#)). The adoption of remote sensing in plant science is promising however the main drawback is the amount and complexity of data collected. To be able to utilize the collected remote sensing data, the machine learning algorithms introduced into the analysis becomes a key technology ([Mahlein, 2016](#); [Fiorani and Schurr, 2013](#)).

#### 1.2 Hyperspectral Imaging and Application

Hyperspectral images capture both spectral and spatial information of a scene. As stated in [Nasrabadi \(2013\)](#), a hyperspectral spectrometer provides hundreds of contiguous bands over a range of the electromagnetic spectrum. An example image cube is shown in Figure 1-1A. As pointed out by [Manolakis and Shaw \(2002\)](#), all materials reflect, absorb, and emit electromagnetic energy at specific wavelengths in distinctive patterns related to their molecular composition. The variation of reflectance or emittance of a material with respect to wavelengths is known as spectral signature. Different materials have different spectral signatures, as shown in Figure 1-1B an example. Exploiting the spectral signatures of different materials enables the detection or identification of target materials in a scene.

Two major applications of hyperspectral imagery based on the ability of distinguishing materials using spectral signatures are classification and target detection. The hyperspectral classification task is to assign class labels for every pixel automatically. The target detection

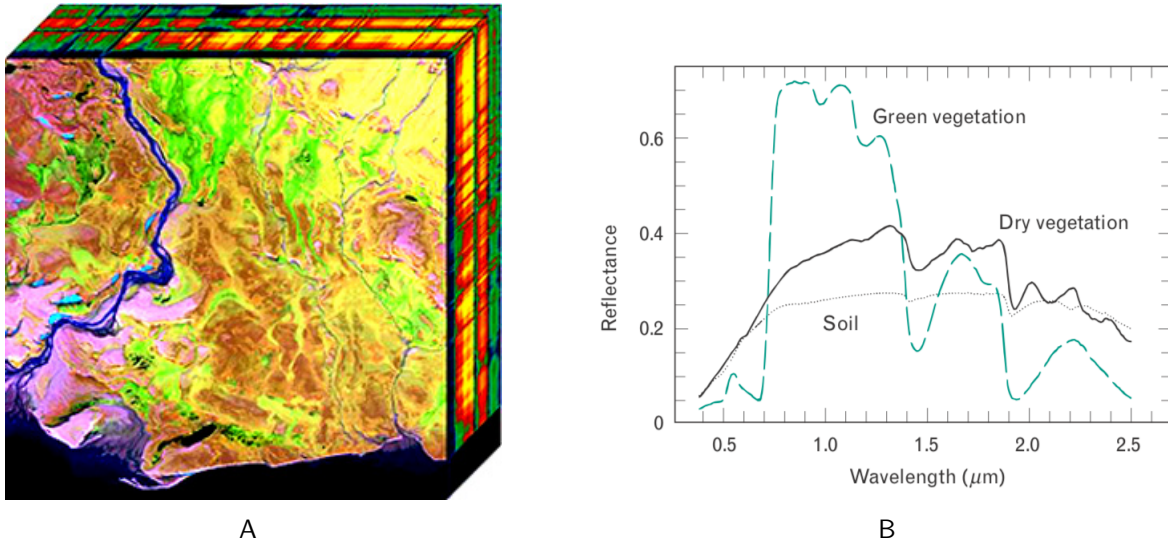


Figure 1-1. Graphic representation of a hyperspectral cube and sample hyperspectral spectra.

A) Graphic representation of hyperspectral data cube ([Commons, 2018](#)); B) Different material produce different reflectance spectra ([Manolakis et al., 2003](#)).

task which can also be considered as a binary classification problem aims at searching pixels for the presence of an interested material ([Manolakis and Shaw, 2002](#)).

Given that spectral signatures potentiate unique characterization of any material, it is appealing to use spectral signatures to identify different materials. However, challenges arise from variations in material surface, atmospheric conditions, location, etc ([Manolakis and Shaw, 2002](#)). And the major ones are from low spatial resolution of the hyperspectral images as well as microscopic material mixing, and multiple scattering such that the measured spectra in a pixel are actually mixtures of spectra. In other words, pixels with pure spectra of single material (pure pixels) rarely exist ([Bioucas-Dias et al., 2012](#)).

### 1.3 Classification in High Dimensional Space

As a representative case of high dimensional data, hyperspectral data suffers from the *Curse of Dimensionality* ([Schürmann, 1996](#)). It is known that, without enough training samples, a classification task would result in less accurate estimation of parameters. As pointed out by [Jain and Waller \(1978\)](#), the optimal dimension of feature vector is limited by the size of training data, i.e. to accurately classify high dimensional data, a large number of training

samples are needed. While in reality the number of training sample is limited; additionally it is time-consuming and computationally expensive to include large amount of training data. The high dimensional space for a given hyperspectral data set is mostly empty so it would be efficient to reduce the dimensionality of the data before classification ([Jain and Waller, 1978](#)).

#### **1.4 Statement of the problem**

Hyperspectral imagery can be used for target material detection because different materials have different spectral signatures. However, the task becomes difficult when trying to classify materials with similar spectral signatures, to be specific, different genotypes of the same plant species. The differences between hyperspectral signatures of different genotypes of switchgrass are not as significant as ones between switchgrass and background materials.

As an example of high dimensional data, hyperspectral data suffered from the *Curse of Dimensionality*. Band selection or feature selection are often applied to hyperspectral data to reduce the dimensionality.

This work examines methods for automated target material detection and dimensionality reduction which enables the classification of materials with similar spectral signatures.

## CHAPTER 2

### LITERATURE REVIEW

This chapter provides reviews existing methods for stitching and making orthomosaics, hyperspectral unmixing and classification in high dimensional space. Stitching and making orthomosaics is a preprocessing step of hyperspectral imagery analysis which gives an overall understanding of the field of interest. Hyperspectral unmixing is a necessary step to address the issue caused by low spatial resolution of hyperspectral sensors causing each pixel to be a mixture of several materials. Hyperspectral imagery is a special case of high-dimensional data, and it shares similar characteristics of general high dimensional data and classification in high dimensional data.

#### 2.1 Stitching and Making Orthomosaics

With unmanned aerial systems becoming popular in applications areas of remote sensing such as military ([DeGarmo, 2004](#); [Ma'Sum et al., 2013](#)) and civil, examples of which are precision agriculture ([Honkavaara et al., 2013](#); [Saari et al., 2011](#)) and biological research ([Bolland-Breen et al., 2015](#)), hyperspectral and thermal imagery have been extensively used and studied.

For the fact that in most cases a large number of images should be taken to cover the whole fields of interest, it is necessary to convert multiple or hundreds of raw scanning images into a single image or a less number of images which is usable and in good quality to be able to represent the earth's surface ([Gross, 2015](#)). As stated in the review of [Szeliski et al. \(2007\)](#), after image capture, the first step in creating orthomosaics is to have a good understanding of the image, i.e. find the suitable mathematical model to describe the motion of the image, and the alignment algorithms that can be applied afterwards. One major alignment algorithm is direct method, which uses pixel-to-pixel matching. Examples of direct methods are hierarchical motion estimation which performs a full search over some range of shifts based on the defined cost function; and Fourier-based alignment based on the properties of Fourier transform. Feature-based methods follow the steps of key-point detection, feature matching, geometric

registration. Another major alignment algorithm is feature based method, where distinctive features are extracted first. In the paper [Zitova and Flusser \(2003\)](#) several detailed feature based methods are discussed. It is argued that feature-based methods are recommended when enough amount of easily detected objects are observed.

As stated in the work of [Mills and McLeod \(2013\)](#), one of the main challenges when creating composite images from aerial photographs is that the quality of scanning images is deteriorated by parallax effects caused by changing in the apparent position of an object viewed. With consideration of this problem, image registration, as explained in the paper [Zitova and Flusser \(2003\)](#), the process of overlaying images of the same scene taken at different times, from different viewpoints, and/or different sensors, is a required step of remote sensing image analysis. There are a number of existing algorithms that are able to automatically align multiple images. One approach is structure from motion, in which the well-known scale invariant feature transform (SIFT) can be used to locate keypoints ([Gross, 2015](#)).

There are also software for stitching and making orthomosaics available such as Pix4Dmapper (Pix4D, S.A., Lausanne, Switzerland), Photoscan (Agisoft LLC, St. Petersburg, Russia), and Microsoft Image Composite Editor (Microsoft, Redmond, Washington, U.S.). As [Gross \(2015\)](#) stated, the choice of software is application dependent: no simple best solution suitable for all cases. Both Pix4Dmapper and Photoscan are commercial software, while Microsoft ICE is a freely available software designed for the application of image stitching. Both Pix4Dmapper and Photoscan have the ability to generate 3D point cloud or 3D images, and options of parameter tuning or including ground control point (GCP) data, while Microsoft ICE focuses solely on panoramic image stitching, with no parameters to tune, nor being able to include additional information apart from images themselves.

## 2.2 Hyperspectral Unmixing

Hyperspectral images are images captured by hyperspectral cameras, which are used to measure electromagnetic energy scattered in their field view in hundreds or thousands of

spectral channels ([Bioucas-Dias et al., 2012](#)). As explained by [Mills and McLeod \(2013\)](#), the signal at one pixel of hyperspectral image is a mixture of light scattered by substances located in field of view. Thus the measured spectra are mixture of spectral of materials in a scene. The spectral signatures of assumed pure materials in the scene are known as endmembers. Unmixing consists of estimating the number of endmembers, getting the spectral signatures as well as their abundances. Unmixing is a common step in hyperspectral imaging based applications.

Unmixing algorithms are categorized based mainly on the type of mixing model assumed, namely linear or nonlinear mixing ([Keshava and Mustard, 2002](#)). For cases in which multiple scattering among distinct endmembers can be ignored and the surface is partitioned according to the fractional abundances, a linear mixture model is suitable to approximate the real mixing situation of every pixel ([Keshava and Mustard, 2002](#)). Despite its subtleties and simplicity, the linear mixing model is indeed an approximation which is acceptable for most of the application.

Geometrical and statistical frameworks are two most used frameworks with the linear mixture model. Geometrical approaches make use of the geometric orientation of hyperspectral data in multidimensional spaces ([Parente and Plaza, 2010](#)). Two main categories of Geometrical based approaches are Pure Pixel based approaches and Minimum Volume based approaches, where Pure Pixel based method is a special case of Minimum Volume based method when the assumption of existence of pure pixel per endmember holds, i.e. the endmembers exist in the original data. Examples of most used algorithms based on Pure Pixel assumption are: pixel purity index algorithm ([Boardman, 1993](#)), N-FINDER ([Winter, 1999](#)), vertex component analysis ([Nascimento and Dias, 2005](#)), simplex growing algorithm ([Chang et al., 2006](#)), etcetera. The pixel purity index algorithm finds the N pixels with highest score of being an extreme after maximum noise fraction (MNF) transformation is applied to the original data as a preprocessing step for reducing dimensionality and boosting signal to noise ratio, with N being a pre-defined value by other algorithms or domain knowledge. The N-FINDER algorithm tries to find the simplex with largest volume from the input hyperspectral

data based on the fact that the endmembers are the vertices of a simplex and the simplex defined by purest pixels is larger than any other simplexes defined by other data from the input hyperspectral data. The vertex component analysis (VCA), also relies on the geometry of convex sets, iteratively projects data onto a direction orthogonal to the subspace spanned by the endmembers already determined until the endmember is exhausted. The new endmember detected every time are the extremes of the projection ([Nascimento and Dias, 2005](#)). Some other algorithms are proposed based on the algorithms mentioned before. For example, the alternating volume maximization, proposed by [Chan et al. \(2011\)](#), is based on N-FINDER, where the maximization of the volume of the simplex is done repeatedly. The successive volume maximization is similar to vertex component analysis where with only the difference of the direction data being projected([Chan et al., 2011](#)).

A general case of geometrical-based approaches are used when the pure pixel constraint does not necessarily hold. Algorithms belong to this class try to find the mixing matrix which minimizes the volume of the simplex defined by the data. The minimum volume transform-nonnegative matrix factorization (MVC-NMF) algorithm solves the minimization problem with a regularization term controlling the volume of simplex ([Miao and Qi, 2007](#)). Similar to MVC-NMF algorithm, the iterative constrained endmembers (ICE) algorithm ([Berman et al., 2004](#)) also solves an optimization problem with regularization, with the sum of squared distances between all the simplex vertices being used as the regularization term ([Bioucas-Dias et al., 2012](#)). On top of the ICE algorithm, [Zare and Gader \(2007\)](#) proposed the sparsity-promoting ICE (SPICE) algorithm, which enables automated number of end member estimation by adding sparsity-promoting priors.

For cases of highly mixed data, the geometrical-based approaches are generally no longer suitable, statistical methods are proposed to use for hyperspectral unmixing problems as statistical inference problems ([Bioucas-Dias et al., 2012](#)). Bayesian approaches, specifically joint maximum a posterior (MAP) estimators ([Bernardo and Smith, 2009](#)), being able to model

statistical variability with priors to have constrained results, are highly used when formulating the unmixing problem.

When a library of pure spectral signatures are available in advance, the unmixing problems are seen as a semi-supervised regression problem of finding a subset of signatures from the library with which every pixel in the input data are modeled (Lordache et al., 2011; Rogge et al., 2006).

### 2.3 Classification in High Dimensional Space

As data has become increasingly larger not only in number of samples, but also in the dimension of feature vectors, especially in applications such as healthcare, remote sensing, image retrieval, etcetera (Yu and Liu, 2003). Although conveying an amount of information, data of high dimensionality may cause problems when applying machine learning algorithms and degrade performance known as the curse of dimensionality.

Ready and Wintz (1973) and Singh and Harrison (1985) proposed the use of well-known dimensionality reduction algorithm, i.e. Principal Component Analysis (PCA), for compression of high dimensional remote sensing data. Green et al. (1988) presents that the Maximum Noise Fraction (MNF) which is a linear transformation that consistently gives images in an order of decreasing quality. Feature selection is considered a process of choosing a subset of original features with original physical meaning retained. Yu and Liu (2003) proposed a fast filter feature selection method which is able to identify relevant features as well as redundancy among relevant features. When considered in the application of hyperspectral imagery, feature selection is also referred to as band selection. Based on whether the desired object information is known, band selection can be categorized to supervised or unsupervised (Yang et al., 2010).

With the focus on the ultimate performance of classification, Jimenez et al. (1998) proposed the use of Projection Pursuit technique, which reduces the dimensionality of data while maintaining as much information as possible by maximizing the separability, which is believed to project the data to a highly separable manifold. Proposed by Hadsell et al. (2006), *Dimensionality Reduction by Learning an Invariant Mapping*, reducing the dimensionality by

learning a mapping, such that "similar" points in the input space will be mapped to nearby points on the learned manifold.

## CHAPTER 3

### MATERIALS AND METHODS

#### 3.1 Dataset

The data used in this work are hyperspectral images collected from two fields of switchgrass in Columbia, Missouri. In one field, a plot-based stand experiment design was adopted, where a group of all the same genotype of switchgrass were planted in a 6 m × 6m plot. And a randomized block design was adopted with five replications in the field. This planting technique is referred to as "Stand" planting (STND). In this field, there are in total 6 genotypes of switchgrass, namely, Liberty, Blackwell, Alamo, Kanlow, Cave in rock (CIR), and Carthage. In the other field, the Genome Wide Association Study (GWAS) is adopted. GWAS is an observational study of a genome-wide set of genetic variants in different individuals to see if any variant is associated with a trait.

A hyperspectral camera mounted on a UAV developed by Headwall Photonics, Inc. was used for the scanning of the fields. The hyperspectral camera has a spectra coverage from 400nm to 1000 nm. In the raw data, 272 bands are observed, and after transforming raw digital indices into reflectance values, 270 bands are kept by the software.

#### 3.2 Switchgrass Detection

To classify the genotypes of switchgrass, the first task is to segment the switchgrass pixels from the images. Hyperspectral unmixing is adopted for switchgrass detection.

##### 3.2.1 Sparsity Promoting Iterated Constrained Endmember Detection (SPICE)

When a linear mixture assumption is adopted, every pixel is considered as a linear combination of the endmembers of the scene ([Berman et al., 2004](#)):

$$X_i = \sum_{k=1}^M p_{ik} E_k + \varepsilon_i, \quad i = 1, \dots, N \quad (3-1)$$

where  $N$  is the number of pixels,  $M$  is the number of endmembers,  $p_{ik}$  is the proportion of endmember  $k$  in pixel  $i$ ,  $E_k$  is the  $k$ th endmember,  $\varepsilon_i$  is an error term. The proportions satisfy

the constraints

$$\sum_{k=1}^M p_{ik} = 1; \quad p_{ik} \geq 0, \quad k = 1, \dots, M \quad (3-2)$$

This model shows that data lie inside a simplex of d-dimensional space and the M endmembers are the vertices of the simplex. In other words, all data are in the simplex constructed by endmembers. A toy example is shown in Figure 3-1. The ICE (Iterated Constrained Endmembers) algorithm tries to minimize residual sum of squares (RSS) between the data and the linear model:

$$RSS = \sum_{i=1}^N (X_i - \sum_{k=1}^M p_{ik} E_k)^T (X_i - \sum_{k=1}^M p_{ik} E_k) \quad (3-3)$$

[Berman et al. \(2004\)](#) further argued that without any constraints there would be more than

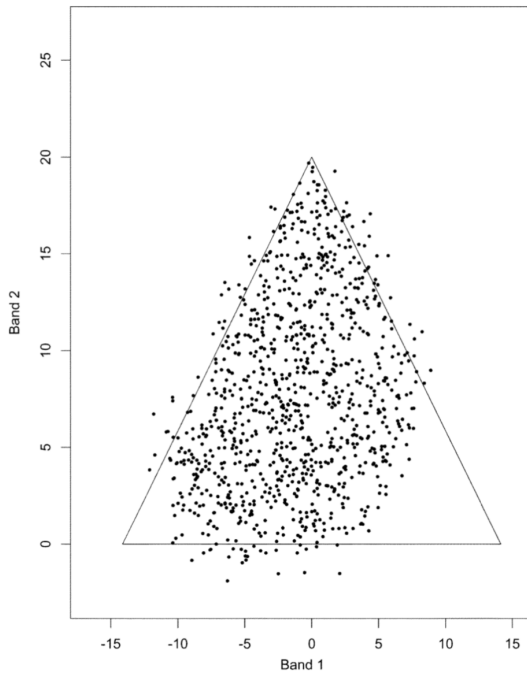


Figure 3-1. Toy example of the data and the simplex shown in two-dimensional space ([Berman et al., 2004](#)).

one minimizer satisfies. So that they proposed adding a sum of squared distances (SSD) term to the objective function to constrain the size of simplex. They proved that the SSD term is equivalent to  $M(M - 1)V$ . In the final form of the proposed objective function shown in Equation 3-4,  $V$  was used instead of  $M(M - 1)V$  to make the objective function approximately

independent of the number of endmembers  $M$ .

$$RSS_{reg} = (1 - \mu) \frac{RSS}{N} + \mu V \quad (3-4)$$

The SPICE algorithm is an extension of the ICE algorithm by adding a sparsity-promoting term to the objective function of ICE algorithm. As described in [Figueiredo \(2003\)](#), this Bayesian approach controls the complexity of model by introducing a Laplacian prior for the parameters of the function to be learned. [Zare and Gader \(2007\)](#) proposed the sparsity-promoting term to be

$$SPT = \sum_{k=1}^M \gamma_k \sum_{i=1}^N |p_{ik}| = \sum_{k=1}^M \gamma_k \sum_{i=1}^N p_{ik} \quad (3-5)$$

where

$$\gamma_k = \frac{\Gamma}{\sum_{i=1}^N p_{ik}} \quad (3-6)$$

The updated objective function with sparsity promotion can be written as

$$RSS_{reg}^* = (1 - \mu) \frac{RSS}{N} + \mu V + SPT \quad (3-7)$$

The iterative optimization procedure used in ICE is still adopted for the optimization in SPICE. The most noticed advantage of this algorithm is that no prior knowledge of the number of endmembers is needed. Setting the initial number of endmembers to a large value, the sparsity-promoting term would indicate those endmembers whose proportion values smaller than the user set threshold to be discarded during the iterative procedure. In this way the number of endmembers is learned automatically. The spectral signatures and the abundance value of every pixel corresponding to every endmember are calculated simultaneously.

### 3.2.2 Switchgrass Detection generation

With detected spectra signatures using SPICE, signatures belong to switchgrass are selected and the corresponding abundance maps are aggregated. The switchgrass pixels are segmented by filtering using a threshold of 0.5 on the abundance maps.

### 3.3 Switchgrass Genotype Classification

#### 3.3.1 Dimensionality Reduction by Learning an Invariant Mapping

For the problem of mapping high dimensional points onto a low dimensional manifold, Hadsell et al. (2006) proposed a nonlinear mapping function given neighborhood relationships between samples in input space. Examples for the source of the neighborhood relationships graph include prior knowledge, manually labeling, etcetera. The algorithm is described as follows: given a set of high dimensional input data points  $\mathcal{I} = \{\vec{X}_1, \dots, \vec{X}_P\}$ , where  $\vec{X}_i \in \mathcal{R}^D$ ,  $\forall i = 1, \dots, n$ , find a parametric function  $G_W : \mathcal{R}^D \rightarrow \mathcal{R}^d$  with  $d \ll D$ , such that simple distance measures in the output space should approximate the neighborhood relationships in the input space. Assume that among the set of high dimensional training points, for each  $\vec{X}_i \in \mathcal{I}$ , there is a set  $S_{\vec{X}_i}$  of training vectors that are deemed to be similar to  $\vec{X}_i$ , with this similarity information coming from prior knowledge. Different from conventional learning systems where the loss function is a sum over all samples, the loss function defined here runs over pairs of samples, known as the contrastive loss function. Let  $\vec{X}_1$  and  $\vec{X}_2 \in \mathcal{I}$  be a pair of input vectors, with  $Y$  being the binary label describing the similarity of this pair of data.  $Y = 0$  if  $\vec{X}_1$  and  $\vec{X}_2$  are deemed similar, and  $Y = 1$  if  $\vec{X}_1$  and  $\vec{X}_2$  are deemed dissimilar. The distance between  $\vec{X}_1$  and  $\vec{X}_2$ , known as  $D_W(\vec{X}_1, \vec{X}_2)$ , written as  $D_W$ , is the distance function to be learned, which is defined as the Euclidean distance between the outputs of  $G_W$ :

$$D_X(\vec{X}_1, \vec{X}_2) = \|G_W(\vec{X}_1) - G_W(\vec{X}_2)\|_2 \quad (3-8)$$

The general form of contrastive loss function is defined as:

$$\mathcal{L}(W) = \sum_{i=1}^P L(W, (Y, \vec{X}_1, \vec{X}_2)^i) \quad (3-9)$$

where  $(Y, \vec{X}_1, \vec{X}_2)^i$  is the  $i$ -th labeled sample pair;  $P$  is the number of training pairs. The contrastive loss function can be further expressed as:

$$\mathcal{L}(W(Y, \vec{X}_1, \vec{X}_2)^i) = (1 - Y)L_S(D_W^i) + YL_D(D_W^i) \quad (3-10)$$

where  $L_S$  is the partial loss function for a pair of similar points;  $L_D$  is the partial loss function for a pair of dissimilar points. For the sake of minimizing  $L$  with respect to  $W$  would result in low values of  $D_W$  for similar pairs of points and high values for dissimilar pairs, the loss function is finally defined as:

$$L(W, Y, \vec{X}_1, \vec{X}_2) = (1 - Y) \frac{1}{2} (D_W)^2 + (Y) \frac{1}{2} \{ \max(0, m - D_W) \}^2 \quad (3-11)$$

where  $m > 0$  is a user-defined margin, which basically defines a radius around  $G_W(\vec{X})$  such that dissimilar pairs contribute to the loss function only if their distance is within this radius. As is illustrated in Figure 3-2A.

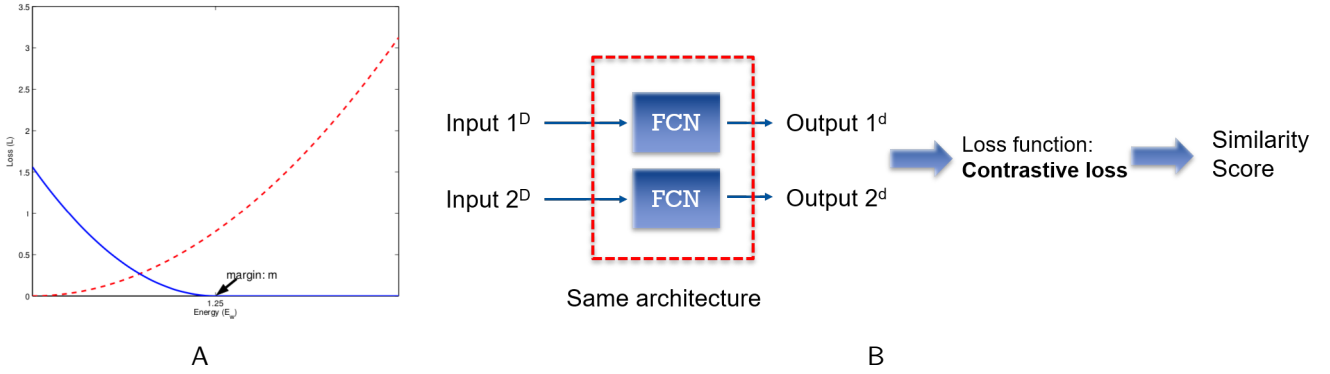


Figure 3-2. Contrastive loss function representation and the network architecture. A) Graph of the loss function  $L$  against the energy  $D_W$ . The dashed (red) line represents the loss function values for the similar pairs and the solid (blue) line represents that for the dissimilar pairs. (Hadsell et al., 2006); B) The network architecture used in this work. It should be noticed that the two networks shown in the figure are actually one; it is shown this way to indicate how the network deal with a pair of inputs separately.

The architecture of the network used in this work is shown in Figure 3-2B. Network with this architecture is also known as the Siamese network, where every single input of the input pairs is processed with exact same network independently

In this work, the neighborhood relationships are obtained from ground truth. To be specific, pixel-level class labels were obtained in advance by manual labeling. During the network training, the pair of pixels belong to same class are considered as similar pair of

points in the original data space, while the pixels belong to different classes of genotype are considered as dissimilar pair of points in the original space.

### 3.3.2 K Nearest Neighbor Classifier

With the original spectra being reduced dimensionality, a multi-class k nearest neighbor classifier is used for classification. K nearest neighbor (KNN) is one of the easiest and most widely used classification algorithms. KNN accomplishes the classification task by first finding the K closest points to every test pixel, and then assign labels by majority vote of these K closest points. The closeness between two points is indeed the similarity between them, which is defined using a distance metric. A popular choice of the distance metric is the Euclidean distance:

$$d(x, x') = \sqrt{(x_1 - x'_1)^2 + \dots + (x_n - x'_n)^2} \quad (3-12)$$

It is interesting to note that KNN is an instance-based algorithm, which means that instead of learning a model, it memorizes the training instances which are afterwards used as knowledge for the prediction of new sample.

### 3.3.3 Ground Truth Generation

Precise pixel level ground truth is needed for the training of the Siamese network as well as the training of the classifier. The pixel level ground truth is generated in a way that is a combination of manually labeling and automated detection. To be specific, the ground truth is first generated by tracing the boundaries of the switchgrass plots, with name of switchgrass genotype assign to every plot. However, some plots are not fully covered with switchgrass. To address this situation, the switchgrass detection described previously is used. The manual labeling is able to get rid of existing false positive pixels from the former switchgrass detection result.

## 3.4 Summary of Proposed Approach

A flowchart including the entire processing approaches is shown in Figure 3-3. Based on the special training technique of the Siamese network - taking pairs of input - the training and

test procedure differ a little. The differences between training and test are indicated in the flowchart using different colors.

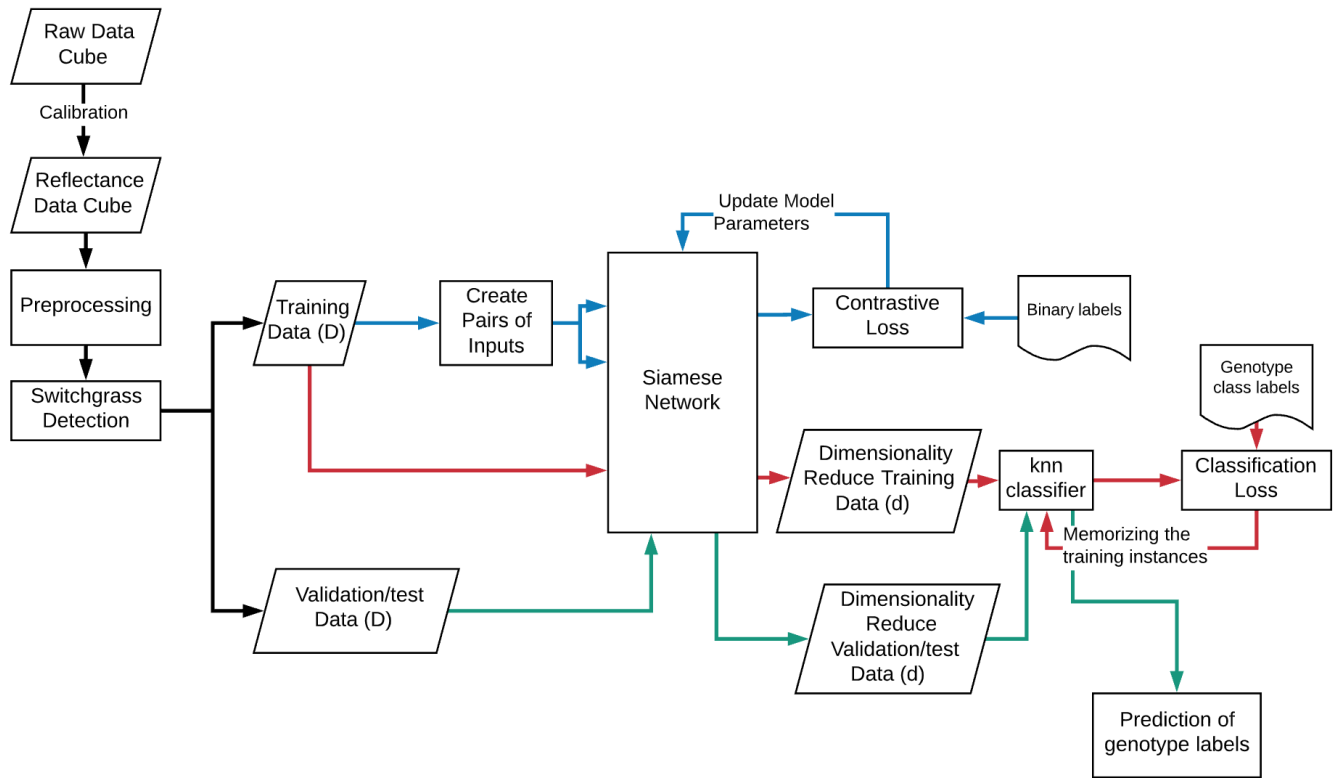


Figure 3-3. The flowchart of the adopted approach. The blue arrows illustrate the training steps of the Siamese network; the red arrows illustrate the training steps of the KNN classifier; the green arrows illustrate the test/validation steps of the Siamese network followed by the KNN classifier. During training of the Siamese network, the input data is always a pair of data points with label either 0 or 1; during test/validation of the Siamese network, the input data is always single data point, and the output is dimensionality reduction result.

## CHAPTER 4 RESULTS

### 4.1 Preprocessing of hyperspectral images

#### 4.1.1 Radiometric Calibration

The hyperspectral images were collected as raw digital numbers so that the conversion from raw hyperspectral data to reflectance cubes is necessary. The raw data cubes are first converted to radiance cubes using dark reference, and then the radiance cubes are converted to reflectance cubes using reference tarps placed in the field during image collection. The SpectralView software (Headwall Photonics, Inc. Boston, United States) was used to generate reflectance cubes and obtaining the spectra of pixels in every hyperspectral image. The reflectance cubes are converted to spectra of every pixel with 270 bands, wavelengths ranging from 396 nm to 996 nm. An example showing the data cube before and after calibration is presented in Figure 4-1.

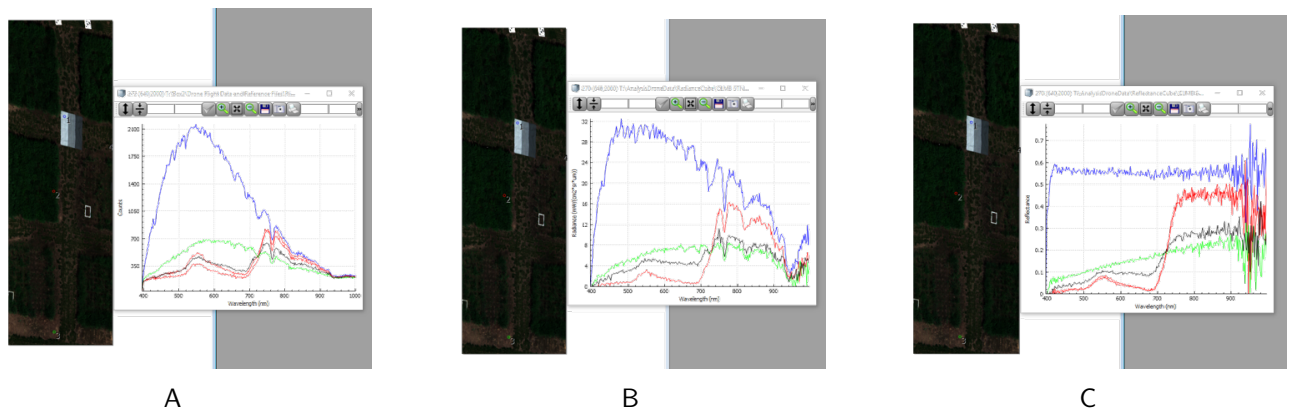


Figure 4-1. Radiometric Calibration. A) Raw data cube opened in the SpectralView software, with the raw digital numbers for 272 wavelengths shown for selected points; B) Radiance date cube opened in the SpectralView software, with calibrated radiance values for 270 bands shown for selected points; C) Reflectance data cube opened in the SpectralView software, with selected spectra shown for selected points. The calibration tarp is also shown in this figure.

#### 4.1.2 Stitching and Making Orthomosaics

Around 40 images were generated during one scan of a field, so ortho-rectification and making a stitched image include all of them would give us a better understanding of the

overview of the whole field, and simultaneously giving suggestions of whether having enough coverage of the field. Shown in Figure 4-2 is an example of orthomosaics made from scanning images from one set of scanning using the SpectralView software. In this example the gaps in between are observed which suggests modifications for the flight plan. Although the further analysis of the data cubes would be on single images instead of analysis of the stitched data cube, this stitched data cube is used in locating every switchgrass plot to assign pixel-level label to the plots.

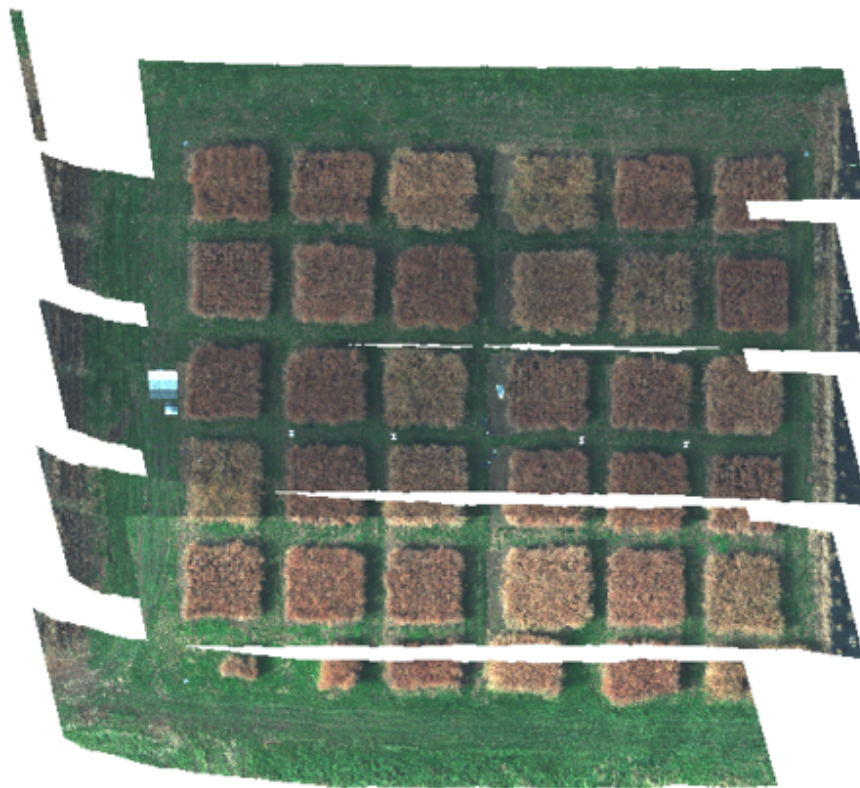


Figure 4-2. Stitched images from one example scanning of the STND switchgrass field.

#### 4.1.3 Noisy Band Removal

Before analysis of spectra, some noisy bands are removed. For the similarity of application as in the work of ([Moghimi et al., 2019](#)), a similar rule of noisy band removal is adopted. The first and last few bands are removed for the fact of high noise (any bands before 430 nm and

after 870 nm). Furthermore, based on ([Moghimi et al., 2018](#)), the bands near  $O_2$  and  $H_2O$  are also removed. In the end, 192 spectral bands out of 270 bands are kept for the upcoming analysis. An example of spectral before and after noisy bands removal is shown in Figure 4-3.

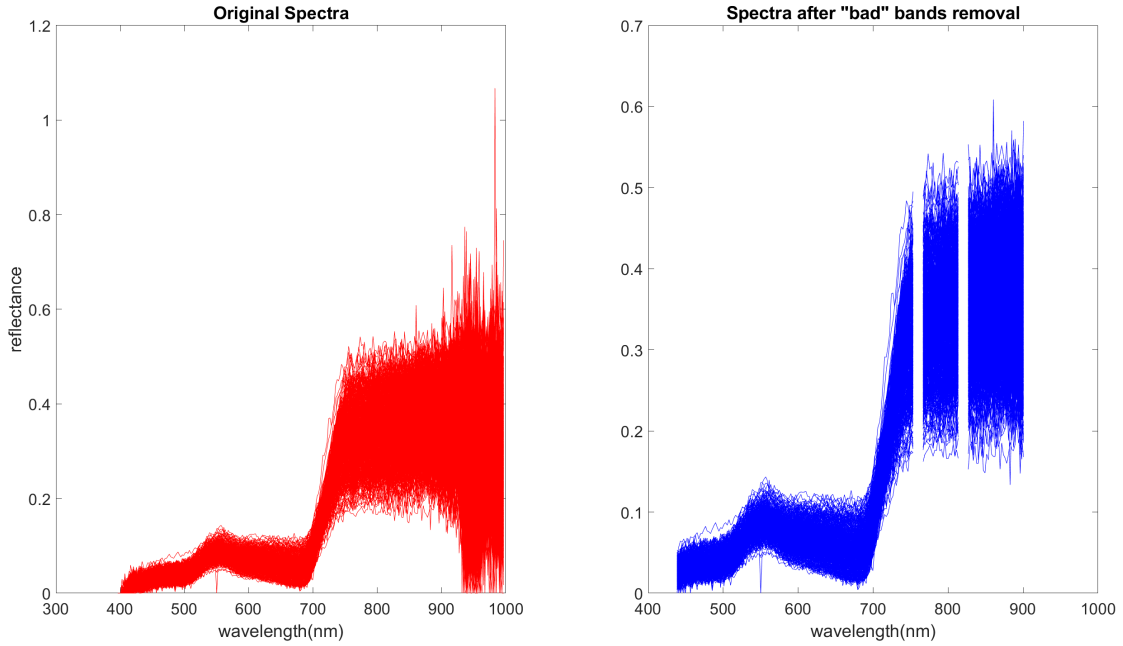


Figure 4-3. Sample spectra before and after noisy band removal.

## 4.2 Detection of Switchgrass

To prepare data for the Siamese Network, the ground truth should be as precise as possible. Human labeling can be precise at boundaries of switchgrass and background, but cannot be precise when several materials are close to each other in a small window, especially when both foreground and background are plants. While the automated detection algorithm can be precise when several small portion of materials presenting to be close to each other. So a combination of these two methods serves a good way for switchgrass detection.

### 4.2.1 Hyperspectral endmember detection and unmixing

Several images considered most representative of all possible endmembers presenting in the scene are selected for endmember detection. Sparsity-Promoting Iterative Constrained Endmembers Detection (SPICE) algorithm is applied for automated endmember detection.

The detected endmembers are then used to unmix all the remaining images and generate abundance maps. The detected endmembers for both of the fields are shown in Figure 4-4.

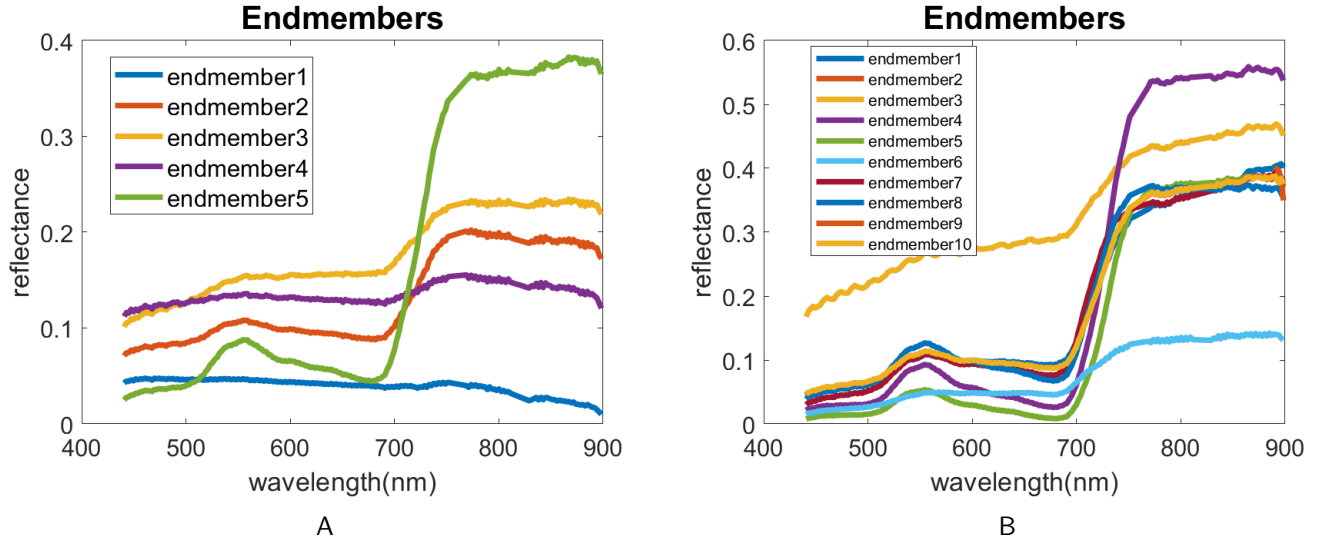


Figure 4-4. Detected endmembers using SPICE algorithm. A) Detected endmembers using SPICE algorithm for the GWAS field; B) Detected endmembers using SPICE algorithm for the STND field.

For the GWAS field, endmember 5 is chosen as the switchgrass endmember, the switchgrass detection result is generated thereby. For the STND field, endmembers 4, 5, and 8 are considered as endmembers for switchgrass, the switchgrass are detected by aggregating abundance maps for the selected endmembers.

#### 4.2.2 Ground truth labeling

With MATLAB programming, the ground-truth labeling is done in an interactive way. As shown in Figure 4-6 as an example, the boundary of every switchgrass plot was traced by cursor, and a number representing the switchgrass class is assigned to this region.

#### 4.2.3 Final detection generation

As mentioned in Chapter 3, the final switchgrass detection results are generated by a combination of automated detection and manual labeling method, i.e. a combination of the aggregated abundance maps and ground truth labeling. A threshold of 0.5 is used to filter the aggregated abundance maps so that most of those pixels which cannot be switchgrass were

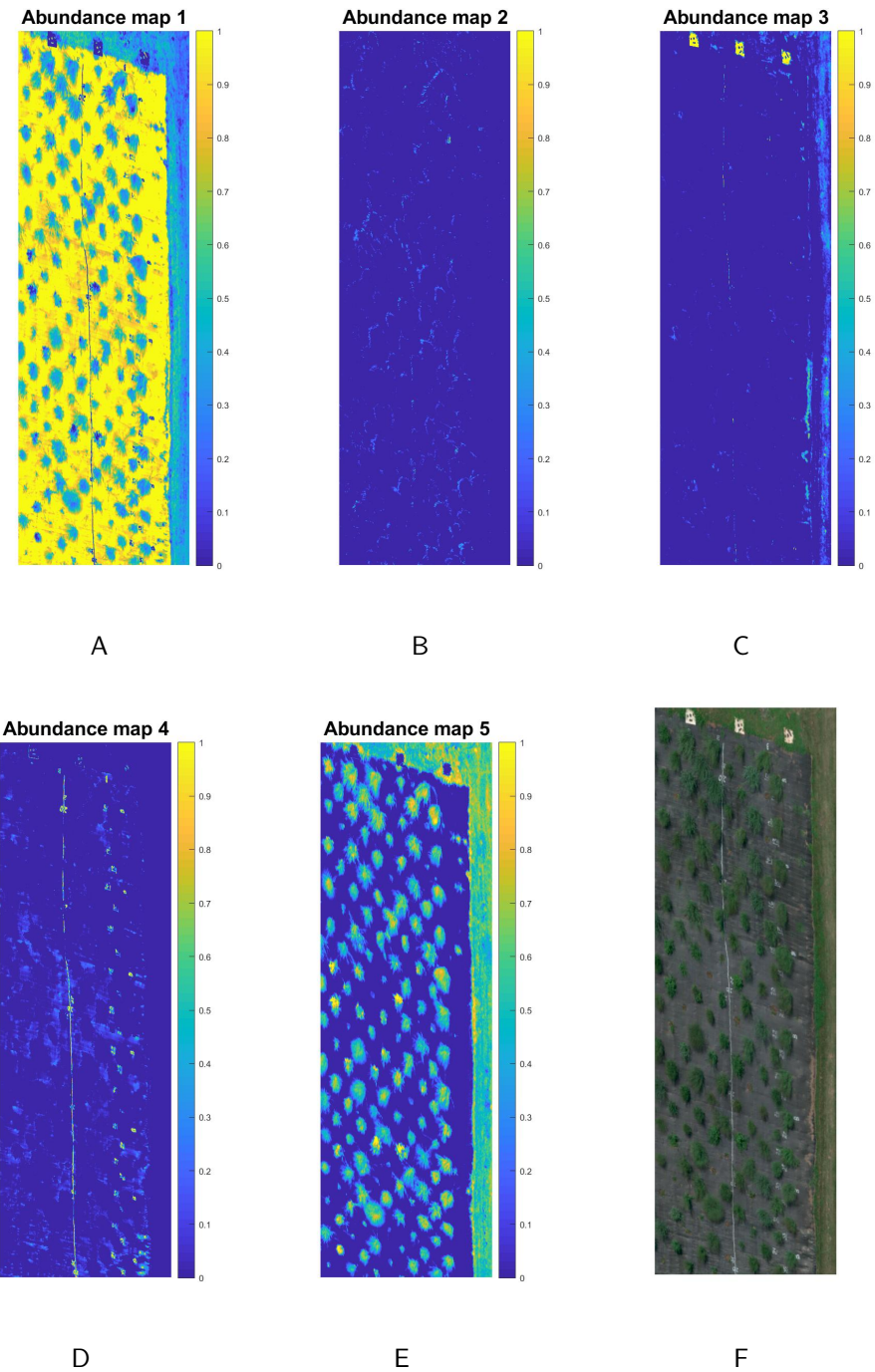
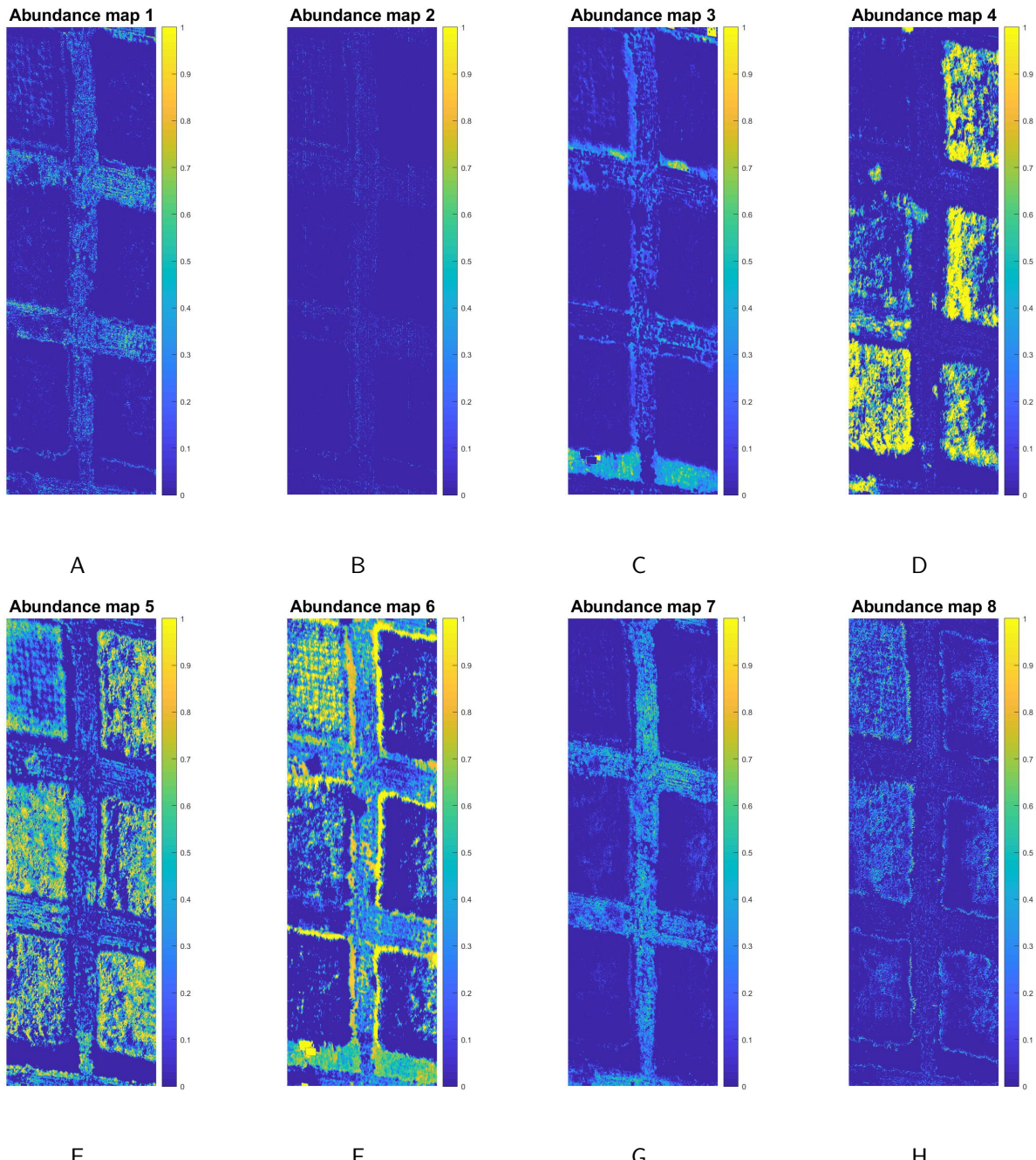


Figure 4-5. Abundance maps and original hyperspectral. A)-E): Abundance maps correspond to detected endmembers for GWAS field; F) Original hyperspectral image visualized with red, green and blue bands.



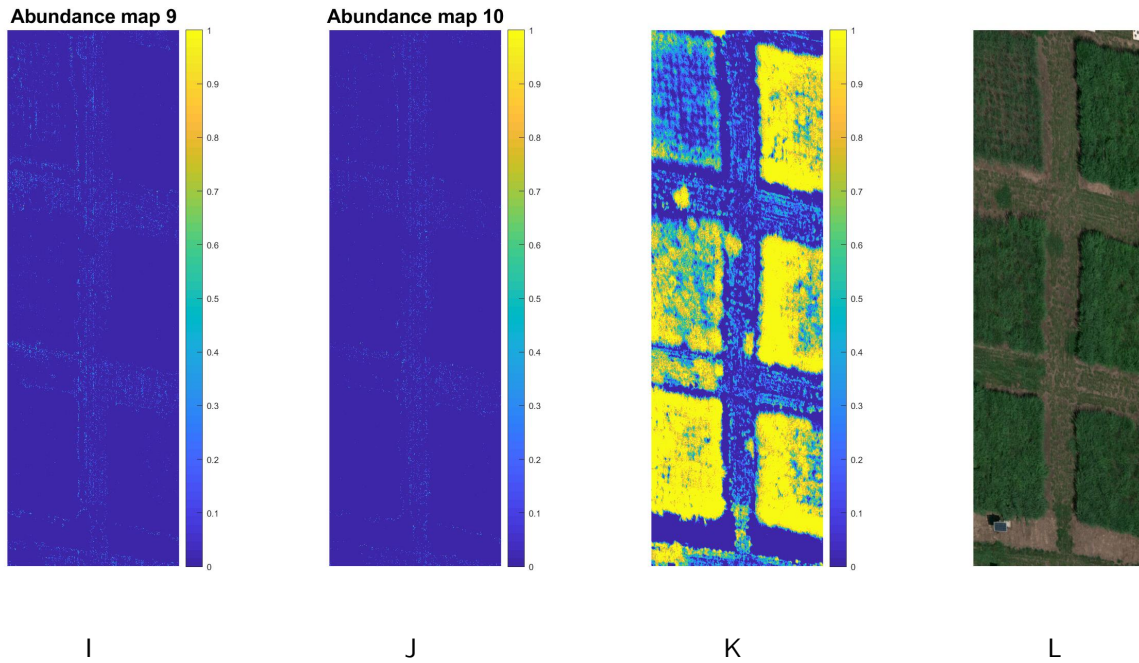


Figure 4-5. Abundance maps and original hyperspectral image for STND field. A)-J) Abundance maps correspond to 10 detected endmembers; K) Aggregated abundance maps correspond to selected endmembers 4, 5, and 8; L) Original hyperspectral image visualized with red, green and blue bands.

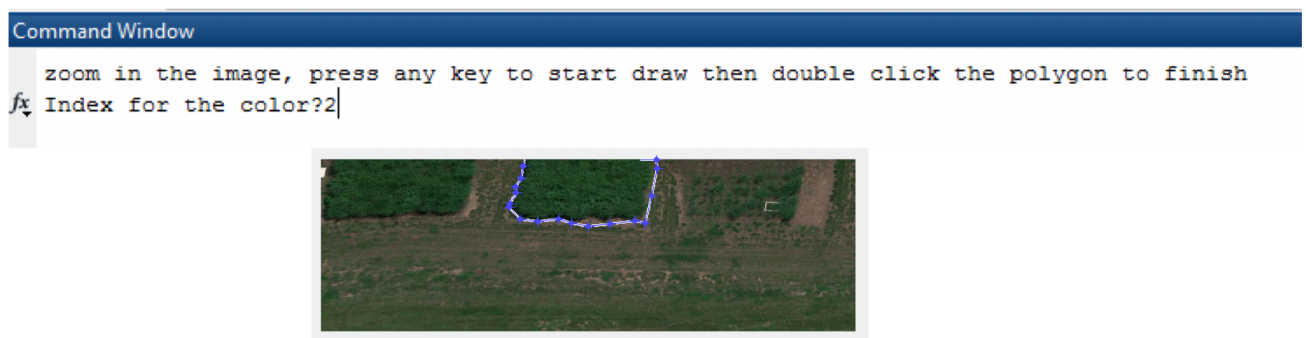


Figure 4-6. Example of manual labeling the ground truth interactively using MATLAB.

discarded; then the manual labeled ground truth is used to generate a ground truth map to filter out those pixels not belonging to the switchgrass plot. Finally these two are combined as the final ground truth which can be used for the training of Siamese network.

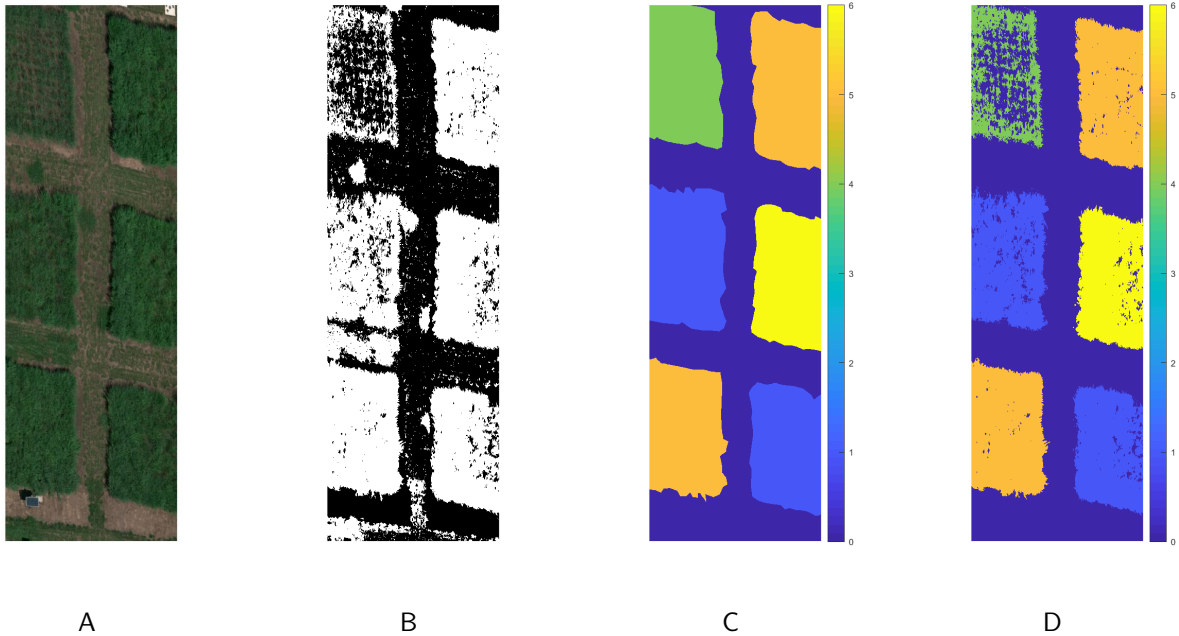


Figure 4-7. A) Original hyperspectral image visualized in RGB space; B) Switchgrass detection result by thresholding the aggregated abundance maps from SPICE unmixing; C) Ground truth generated by manual labeling; D) Final switchgrass detection result by combining results of B) and C).

### 4.3 Switchgrass Classification Results

The classification task is split into two parts: dimensionality reduction with the Siamese network, and classification using k-nearest neighbor. A cross-validation is designed to show the generalization of the network: several images were chosen as training images, the other images were used as test images. Every fold of experiment is designed to randomly select 12 images as training images, to be specific, 2 images are randomly selected from every switchgrass class every time, to ensure that the training data are not hand selected. Furthermore, with selected images, the check of class number balance is done before model training. For classes having insufficient training samples, the over-sampling method called Synthetic Minority

Over-sampling Technique (SMOTE) ([Chawla et al., 2002](#)) is used to generate artificial samples. Only spectra for switchgrass pixels are included in the classification task.

#### 4.3.1 Siamese Network Training

Fully connected neural network is used for both architectures of the Siamese network, with the number of neurons of the last layer set to be the number of dimension to keep. The training images are further devided into three parts: training, validation and test. The validation set is used to tune the parameters of the Siamese model, the test set is used to evaluate the model performance.

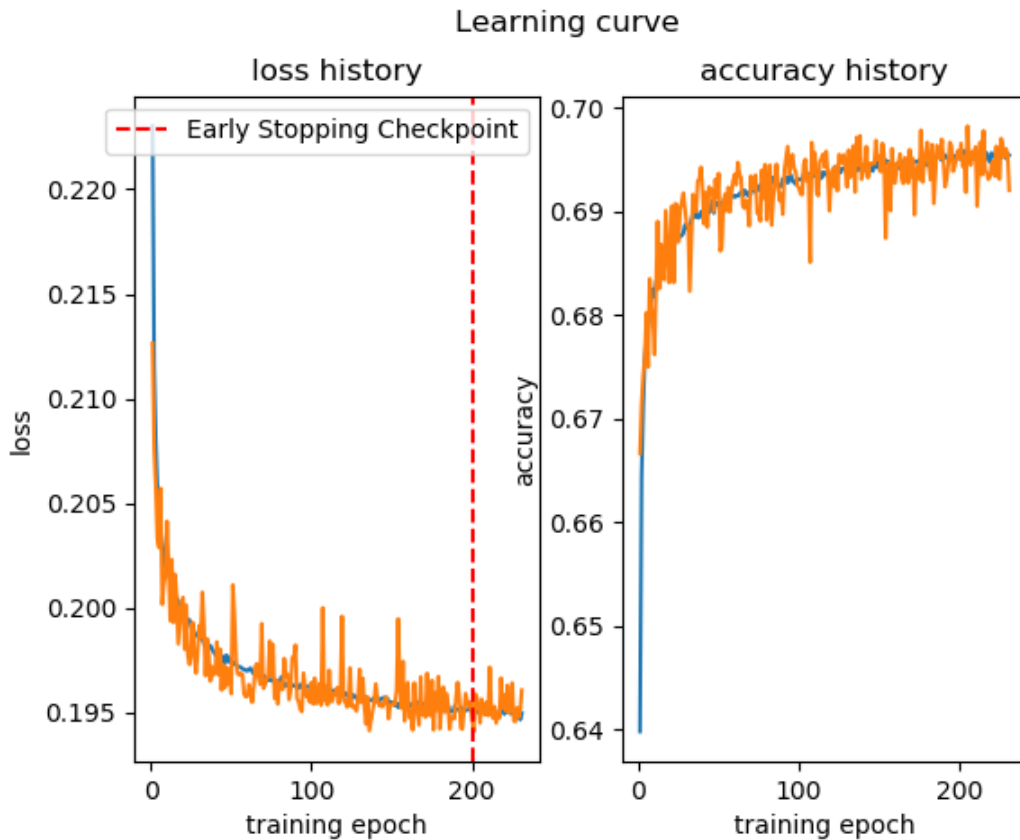


Figure 4-8. Learning curve for Siamese network training. An early stop check based on the validation loss was adopted to monitor the training process and stop training when there is no improvement of the network performance.

#### 4.3.2 Classification

With the dimensionality reduction network (Siamese network) trained, the dimensionality reduced spectra are input to the multi-class k-nearest neighbor (knn) classification model. The number of dimension kept is evaluated by classification accuracy based on the cross-validation experiments. Five-nearest neighbor is adopted. The same set of training data is used to train the model.

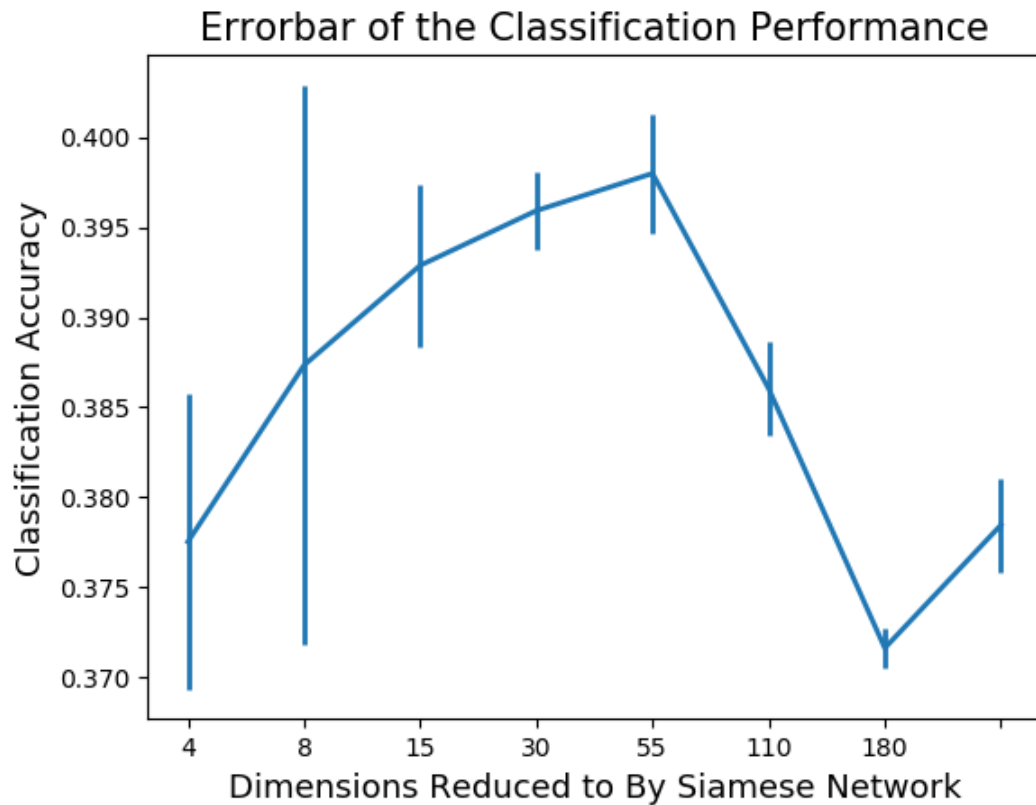


Figure 4-9. Errorbar of classification performance versus the number of dimensions kept.

The final classification performance was evaluated with receiver operating characteristic (ROC) curves and confusion matrices, as well as visualizations on top of the original images.

To show that the performance of this model is consistent regardless of the training data, an experiment is done first showing the overall validation accuracy for every fold. The result is shown in Table 4-1.

Table 4-1. Average classification accuracy of training folds. As described previously, the training data were chosen randomly for every fold.

Fold	1	2	3	4	5	6	7	8
Average classification accuracy	0.3705	0.3709	0.3948	0.3668	0.3785	0.3860	0.3773	0.3767

Learning from Table 4-1 and Figure 4-9, conclusion can be drawn that even with randomly selected training images, the overall performance would remain consistent with a small variance. Different numbers dimensionality kept are also experimented with cross validation to find an optimal dimensionality to reduce to. The classification accuracy is used as the evaluation metric. As shown in Figure 4-9, using Siamese network to reduce the dimensionality to either 30 or 55 yield comparatively good classification result with a small variance. The overall classification performance, i.e. ROC curves and confusion matrix and selected classification result shown on images are shown below. In Figure 4-10, the classification performance of test data selected from training images are shown; in Figure 4-11, the overall classification performance of all test images are shown; and in Figure 4-12, the classification results are shown in images comparing to the ground truth.

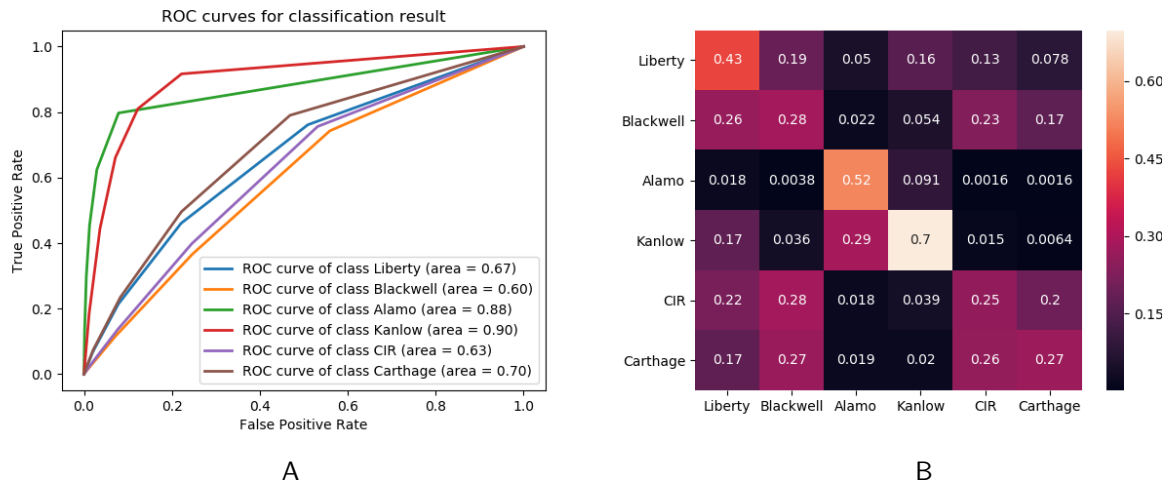


Figure 4-10. A) The classification performance for all switchgrass pixels for all test data selected from training images evaluated by ROC curves; B) The final classification performance for all switchgrass pixels for all test data selected from training images evaluated by confusion matrix.

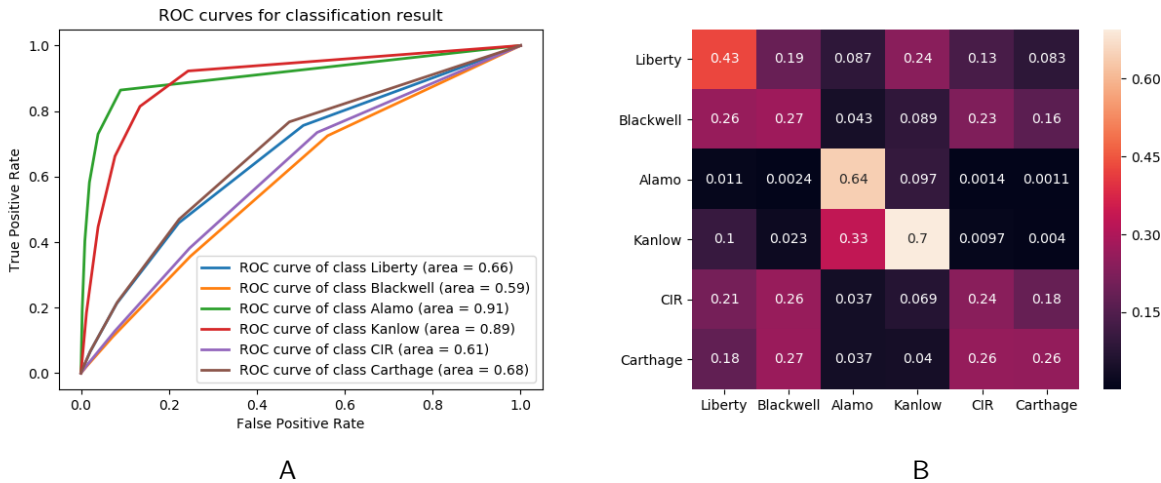


Figure 4-11. A) The final classification performance for all switchgrass genotypes for all test images evaluated by ROC curves; B) The final classification performance for all switchgrass genotypes for all test images evaluated by confusion matrix.

Referring to the classification results shown in Figure 4-10 and Figure 4-11, conclusion is drawn that switchgrass genotypes Alamo and Kanlow have better classification performance compared to other genotypes. And the switchgrass genotype having the third best classification performance is Liberty. The other three genotypes Carthage, CIR and Blackwell do not have satisfactory results - they tend to be mis-classified to anyone of the three with almost equal ratios. To examine the cause of the result, the original spectra for all genotypes and the results of dimensionality reduction are checked and the mean and variances are shown for every genotype. As can be seen from Figure 4.3.2, the spectra of Alamo, Kanlow and Liberty are more separable, while the spectra of Carthage, CIR and Blackwell appear close to each other and with a large variance. Although the mean value for Liberty is different from others, the separability of it is believed to be degraded. As can be observed from the figure, the variances of the Carthage, CIR and Blackwell's spectra are so large that the spectral of Liberty are included inside their distribution. The outputs of dimensionality reduction shown in Figure 4-12A and Figure 4-12B explain the final classification performance: the Siamese network learns a mapping to a manifold where the representations for Blackwell, CIR and Carthage are

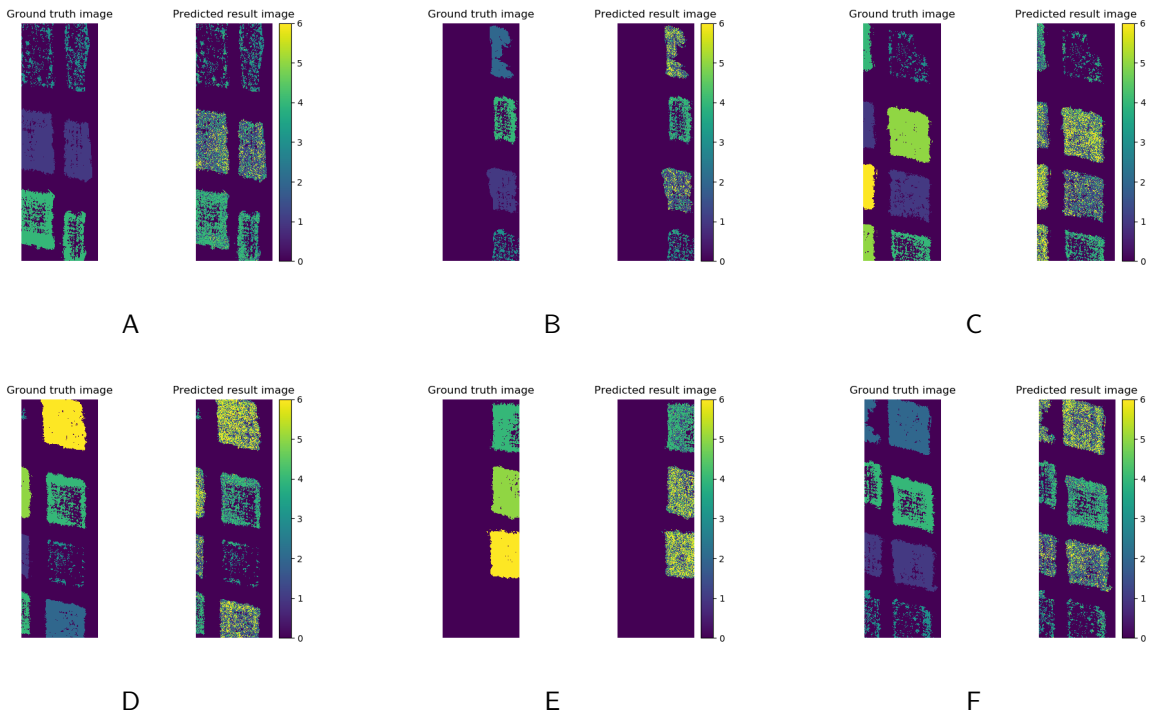
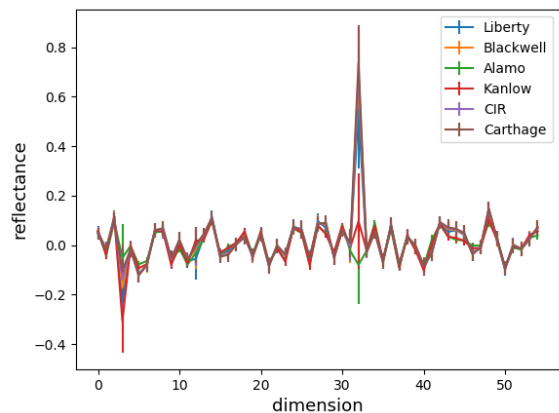
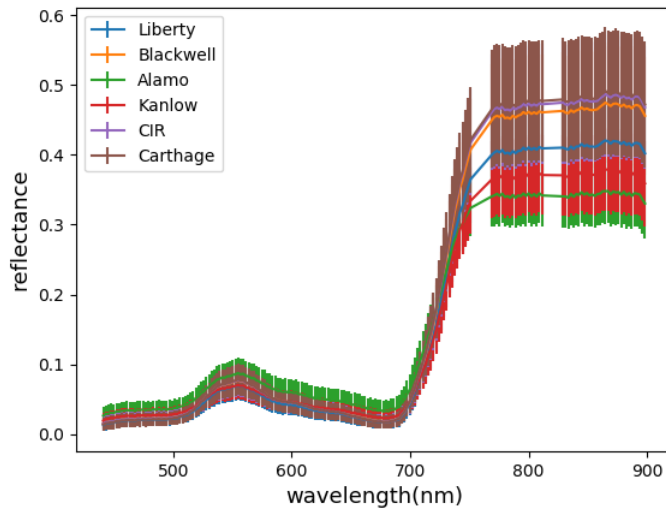


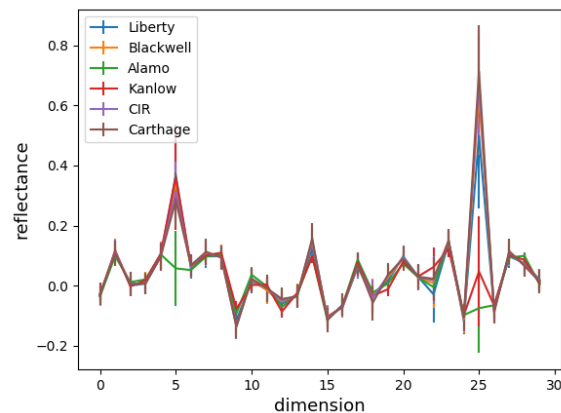
Figure 4-12. Sample classification result shown in images. Different colors represent different genotypes of switchgrass. 1: Liberty; 2: Blackwell; 3: Alamo; 4: Kanlow; 5: Cave in rock (CIR); 6: Carthage.

similar to each other, while the representations for Kanlow and Alamo show some separability. This observation coincide with the classification results.

It is interesting to find that all three switchgrass genotypes perform better in classification are lowland switchgrass. The other three genotypes are upland switchgrass. As mentioned previously, for these three lowland switchgrass genotypes, Alamo and Kanlow perform better in classification than Liberty, which can be explained that for both Alamo and Kanlow, they died during the winter season and green up later than other genotypes in the spring.



A



B

Figure 4-12. Original spectra and dimensionality reduction result of Siamese network. A) Original spectra for 6 switchgrass genotypes, with the variances shown in the error bars; B) Dimensionality reduction result of Siamese network with 55 neurons in last layer; C) Dimensionality reduction result of Siamese network with 30 neurons in last layer

## CHAPTER 5

### SUMMARY AND CONCLUSIONS

An automated hyperspectral imagery processing protocol is first created before digging into algorithm development. With necessary data preprocessing done, dimensionality reduction and classification are performed successively. Main algorithms involved are Sparsity Promoting Iterated Constrained Endmember (SPICE) algorithm and Dimensionality Reduction by Learning an Invariant Mapping (Siamese network).

The Sparsity Promoting Iterated Constrained Endmember (SPICE) algorithm is proved to be a powerful automated hyperspectral endmember detection method for the problem presented in this work. Unmixing with the detected endmembers enables the switchgrass pixel detection task.

Owning to the fact that the difference between different genotypes of switchgrass are not large enough, i.e. not as large as the difference between switchgrass and the background, using only SPICE would not be enough for genotype classification. Additionally, knowing that the performance for high-dimensional data would be degenerated resulting from the curse of dimensionality. The Dimensionality Reduction by Learning an Invariant Mapping algorithm is considered an ideal dimensionality reduction algorithm which would boost the classification performance simultaneously. The Siamese network takes pairs of inputs together to learn a mapping from the high dimension to a low one, such that in the low dimensional representations of the same class are close to each other while points from different classes are far away from each other. With the fact that multi-class classification being a difficult task, this method presents a reasonable result. There are several reasons for not having satisfactory results:

Not having enough training pairs from belong to different classes when train the Siamese network. For the training step, the Siamese network takes a pair of inputs every time, either from same class or from different classes, which means classes 1 and 2, classes 1 and 3, classes 1 and 4, classes 1 and 5, classes 1 and 6 are all considered as from different classes. This

situation results in the need of much more pairs of samples to be able to distinguish every class from any other five classes. As can also be learned from the dimensionality reduction outputs which did not show the desired separability.

Not having enough training samples for the K-nearest neighbor classifier. KNN is an instance-based algorithm, in other words more training samples provided would provide much knowledge for the model make better prediction for the test data.

The original images appear in different lighting conditions, which would lead to the issue that spectra belong to same class from different images would differ. This is also the reason for the original spectra having a large variance.

Based on the analysis of unsatisfactory of current results and the limitations of current method, some potential future works are proposed.

Classify the points in a one-versus-all way, instead of the one-versus-one way adopted here. One-versus-all classification predicts every data point with a binary classifier every time and the results are combined to generate final results.

Include more training samples for the KNN classifier training. Alternatively, classifiers which are not instance-based can be adopted.

If use other classifiers, it is recommended to jointly train the Siamese network and the classifier to guarantee the Siamese network learn a desired mapping which separates data points from different classes and gathers together data points from same class.

## REFERENCES

- Berman, Mark, Kiiveri, Harri, Lagerstrom, Ryan, Ernst, Andreas, Dunne, Rob, and Huntington, Jonathan F. "ICE: A statistical approach to identifying endmembers in hyperspectral images." *IEEE transactions on Geoscience and Remote Sensing* 42 (2004).10: 2085–2095.
- Bernardo, José M and Smith, Adrian FM. *Bayesian theory*, vol. 405. John Wiley & Sons, 2009.
- Bioucas-Dias, José M, Plaza, Antonio, Dobigeon, Nicolas, Parente, Mario, Du, Qian, Gader, Paul, and Chanussot, Jocelyn. "Hyperspectral unmixing overview: Geometrical, statistical, and sparse regression-based approaches." *IEEE journal of selected topics in applied earth observations and remote sensing* 5 (2012).2: 354–379.
- Boardman, Joseph W. "Automating spectral unmixing of AVIRIS data using convex geometry concepts." (1993).
- Bolland-Breen, Barbara, Brooks, John D, Jones, Matthew RL, Robertson, John, Betschart, Sonja, Kung, Olivier, Cary, S Craig, Lee, Charles K, and Pointing, Stephen B. "Application of an unmanned aerial vehicle in spatial mapping of terrestrial biology and human disturbance in the McMurdo Dry Valleys, East Antarctica." *Polar biology* 38 (2015).4: 573–578.
- Chan, Tsung-Han, Ma, Wing-Kin, Ambikapathi, ArulMurugan, and Chi, Chong-Yung. "A simplex volume maximization framework for hyperspectral endmember extraction." *IEEE Transactions on Geoscience and Remote Sensing* 49 (2011).11: 4177–4193.
- Chang, C-I, Wu, C-C, Liu, Weimin, and Ouyang, Y-C. "A new growing method for simplex-based endmember extraction algorithm." *IEEE Transactions on Geoscience and Remote Sensing* 44 (2006).10: 2804–2819.
- Chawla, Nitesh V, Bowyer, Kevin W, Hall, Lawrence O, and Kegelmeyer, W Philip. "SMOTE: synthetic minority over-sampling technique." *Journal of artificial intelligence research* 16 (2002): 321–357.
- Commons, Wikimedia. "File:HyperspectralCube.jpg — Wikimedia Commons, the free media repository." 2018. [Online; accessed 19-September-2019].  
URL <https://commons.wikimedia.org/w/index.php?title=File:HyperspectralCube.jpg&oldid=299520270>
- DeGarmo, Matthew T. "Issues concerning integration of unmanned aerial vehicles in civil airspace." *Center for Advanced Aviation System Development* 4 (2004).
- Figueiredo, Mário AT. "Adaptive sparseness for supervised learning." *IEEE transactions on pattern analysis and machine intelligence* 25 (2003).9: 1150–1159.
- Fiorani, Fabio and Schurr, Ulrich. "Future scenarios for plant phenotyping." *Annual review of plant biology* 64 (2013): 267–291.

- Green, Andrew A, Berman, Mark, Switzer, Paul, and Craig, Maurice D. "A transformation for ordering multispectral data in terms of image quality with implications for noise removal." *IEEE Transactions on geoscience and remote sensing* 26 (1988).1: 65–74.
- Gross, John W. "A comparison of orthomosaic software for use with ultra high resolution imagery of a wetland environment." *Center for Geographic Information Science and Geography Department, Central Michigan University, Mt. Pleasant, MI, USA. Available from: [http://www.imagin.org/awards/sppc/2015/papers/john\\_gross\\_paper.pdf](http://www.imagin.org/awards/sppc/2015/papers/john_gross_paper.pdf)* (2015).
- Hadsell, Raia, Chopra, Sumit, and LeCun, Yann. "Dimensionality reduction by learning an invariant mapping." *2006 IEEE Computer Society Conference on Computer Vision and Pattern Recognition (CVPR'06)*. vol. 2. IEEE, 2006, 1735–1742.
- Honkavaara, Eija, Saari, Heikki, Kaivosoja, Jere, Pölönen, Ilkka, Hakala, Teemu, Litkey, Paula, Mäkinen, Jussi, and Pesonen, Liisa. "Processing and assessment of spectrometric, stereoscopic imagery collected using a lightweight UAV spectral camera for precision agriculture." *Remote Sensing* 5 (2013).10: 5006–5039.
- Iordache, Marian-Daniel, Bioucas-Dias, José M, and Plaza, Antonio. "Sparse unmixing of hyperspectral data." *IEEE Transactions on Geoscience and Remote Sensing* 49 (2011).6: 2014–2039.
- Jain, Anil K and Waller, William G. "On the optimal number of features in the classification of multivariate Gaussian data." *Pattern recognition* 10 (1978).5-6: 365–374.
- Jimenez, Luis O, Landgrebe, David A, et al. "Supervised classification in high-dimensional space: geometrical, statistical, and asymptotical properties of multivariate data." *IEEE Transactions on Systems, Man, and Cybernetics, Part C: Applications and Reviews* 28 (1998).1: 39–54.
- Keshava, Nirmal and Mustard, John F. "Spectral unmixing." *IEEE signal processing magazine* 19 (2002).1: 44–57.
- Mahlein, Anne-Katrin. "Plant disease detection by imaging sensors—parallels and specific demands for precision agriculture and plant phenotyping." *Plant disease* 100 (2016).2: 241–251.
- Manolakis, Dimitris, Marden, David, Shaw, Gary A, et al. "Hyperspectral image processing for automatic target detection applications." *Lincoln laboratory journal* 14 (2003).1: 79–116.
- Manolakis, Dimitris and Shaw, Gary. "Detection algorithms for hyperspectral imaging applications." *IEEE signal processing magazine* 19 (2002).1: 29–43.
- Ma'Sum, M Anwar, Arrofi, M Kholid, Jati, Grafika, Arifin, Futuhal, Kurniawan, M Nanda, Mursanto, Petrus, and Jatmiko, Wisnu. "Simulation of intelligent unmanned aerial vehicle (uav) for military surveillance." *2013 International Conference on Advanced Computer Science and Information Systems (ICACSIS)*. IEEE, 2013, 161–166.

- Miao, Lidan and Qi, Hairong. "Endmember extraction from highly mixed data using minimum volume constrained nonnegative matrix factorization." *IEEE Transactions on Geoscience and Remote Sensing* 45 (2007).3: 765–777.
- Mills, Steven and McLeod, Philip. "Global seamline networks for orthomosaic generation via local search." *ISPRS journal of photogrammetry and remote sensing* 75 (2013): 101–111.
- Moghimi, Ali, Yang, Ce, and Anderson, James A. "Aerial hyperspectral imagery and deep neural networks for high-throughput yield phenotyping in wheat." *arXiv preprint arXiv:1906.09666* (2019).
- Moghimi, Ali, Yang, Ce, Miller, Marisa E, Kianian, Shahryar, and Marchetto, Peter. "A novel approach to assess salt stress tolerance in wheat using hyperspectral imaging." *Frontiers in plant science* 9 (2018): 1182.
- Nascimento, José MP and Dias, José MB. "Vertex component analysis: A fast algorithm to unmix hyperspectral data." *IEEE transactions on Geoscience and Remote Sensing* 43 (2005).4: 898–910.
- Nasrabadi, Nasser M. "Hyperspectral target detection: An overview of current and future challenges." *IEEE Signal Processing Magazine* 31 (2013).1: 34–44.
- Parente, Mario and Plaza, Antonio. "Survey of geometric and statistical unmixing algorithms for hyperspectral images." *2010 2nd Workshop on Hyperspectral Image and Signal Processing: Evolution in Remote Sensing*. IEEE, 2010, 1–4.
- Ready, P and Wintz, P. "Information extraction, SNR improvement, and data compression in multispectral imagery." *IEEE Transactions on communications* 21 (1973).10: 1123–1131.
- Rogge, Derek M, Rivard, Benoit, Zhang, Jinkai, and Feng, Jilu. "Iterative spectral unmixing for optimizing per-pixel endmember sets." *IEEE Transactions on Geoscience and Remote Sensing* 44 (2006).12: 3725–3736.
- Saari, Heikki, Pellikka, Ismo, Pesonen, Liisa, Tuominen, Sakari, Heikkilä, Jan, Holmlund, Christer, Mäkinen, Jussi, Ojala, Kai, and Antila, Tapani. "Unmanned Aerial Vehicle (UAV) operated spectral camera system for forest and agriculture applications." *Remote Sensing for Agriculture, Ecosystems, and Hydrology XIII*. vol. 8174. International Society for Optics and Photonics, 2011, 81740H.
- Schürmann, Jürgen. "Pattern classification: a unified view of statistical and neural approaches." (1996).
- Singh, Ashbindu and Harrison, Andrew. "Standardized principal components." *International journal of remote sensing* 6 (1985).6: 883–896.
- Szeliski, Richard et al. "Image alignment and stitching: A tutorial." *Foundations and Trends® in Computer Graphics and Vision* 2 (2007).1: 1–104.

- Winter, Michael E. "N-FINDR: An algorithm for fast autonomous spectral end-member determination in hyperspectral data." *Imaging Spectrometry V*. vol. 3753. International Society for Optics and Photonics, 1999, 266–275.
- Yang, He, Du, Qian, Su, Hongjun, and Sheng, Yehua. "An efficient method for supervised hyperspectral band selection." *IEEE Geoscience and Remote Sensing Letters* 8 (2010).1: 138–142.
- Yu, Lei and Liu, Huan. "Feature selection for high-dimensional data: A fast correlation-based filter solution." *Proceedings of the 20th international conference on machine learning (ICML-03)*. 2003, 856–863.
- Zare, Alina and Gader, Paul. "Sparsity promoting iterated constrained endmember detection in hyperspectral imagery." *IEEE Geoscience and Remote Sensing Letters* 4 (2007).3: 446–450.
- Zitova, Barbara and Flusser, Jan. "Image registration methods: a survey." *Image and vision computing* 21 (2003).11: 977–1000.

## BIOGRAPHICAL SKETCH

Hudanyun Sheng received her Bachelor of Science degree in Physics from Tongji University in 2015. She entered the graduate school in University of Florida to graduate with her Master of Science degree in Industrial and Systems Engineering and Electrical and Computer Engineering, in 2017 and 2019, respectively.